한국전산구조공학회
2002년도 가을 학술발표회 논문집

레이저 화선의 모델링

Simple Modeling for Laser Scribing

정 철 섭 *
Chung , Chulsup

ABSTRACT

Accurately controlling the shape of the read/write head structure is critical in the performance of a modern hard disk drive. The sliders investigated are composed of alumina and titanium carbide (AlTiC) and act as an air bearing when passing over the disks. Controlling the curvature of the slider is of primary importance. A laser scribing system that produces curvature by inducing residual stress into the slider can be utilized. Predicting the curvature created by a pattern of scribes is of great importance to increase the control over the sliders' shape. Using finite element analysis a force system that produces stresses similar to the laser scribing is applied. The curvatures created by the force system are calibrated to experimental measurements.

1. Introduction

In a modern hard disk drive, the flying height of the read/write head is one of the primary influences on data storage density and hard drive speed. The read/write head is contained within a slider that acts as an air bearing. Therefore the shape of the slider directly determines the flying height of the read/write head. The flying height in modern hard drives has dropped below 25 nanometers; thus accurate control of the slider's shape is necessary to increase performance (Tam). Controlling this shape is very demanding – the peak-to-valley deflections of the slider are on the order of nanometers.

Laser scribing is a newer technique for controlling the shape of sliders. Figure 1 illustrates the simple technique: a pulsed laser is focused on the surface of the ceramic slider, and with sufficient power input a small circle of material is melted. The solidification of these material results in a localized stress around the circle-the ceramic shrinks as it solidifies and the material outside the dot is placed in tension. If a line of dots is created, the spacing between the dots can be decreased until it resembles a solid line. Studies at IBM have shown that as the dot spacing is decreased, the resulting deflection saturates, producing a continuous, repeatable "scribe" (Tam, et. al. (1999)).

These laser scribes produce appreciable curvature in the both directions relative to the scribe axis. These curvatures are of the same order of magnitude and in the same direction (shown in Figure 2). This effect can be used to produce nanometer-scale shape changes that can be useful in manufacturing applications such as disk read-write heads. The objective of this research is to develop a model for laser scribing processes used in the manufacture of hard disk drive heads. Such a model would allow theoretical determination of a scribing pattern that would produce a desired shape, without resulting to tedious experiments to determine the effects of various scribe geometries. Also, with a well-developed model, the system could be used to flatten sliders that already contained too much deflection or to remove asymmetries in the shape of the slider while producing the final shape desired by the designers. The model uses the plate theory to approximate the scribe- induced stresses. Scribing experiments were made to verify the accuracy of the model.

* 정회원 건양대학교 기계공학과 부교수

2. Problem Description

The sliders are constructed of an alumina-titanium carbide (AlTiC) ceramic, and are approximately 1.25 mm by 1.07 mm by 0.30 mm (this size is know as the "pico" slider).

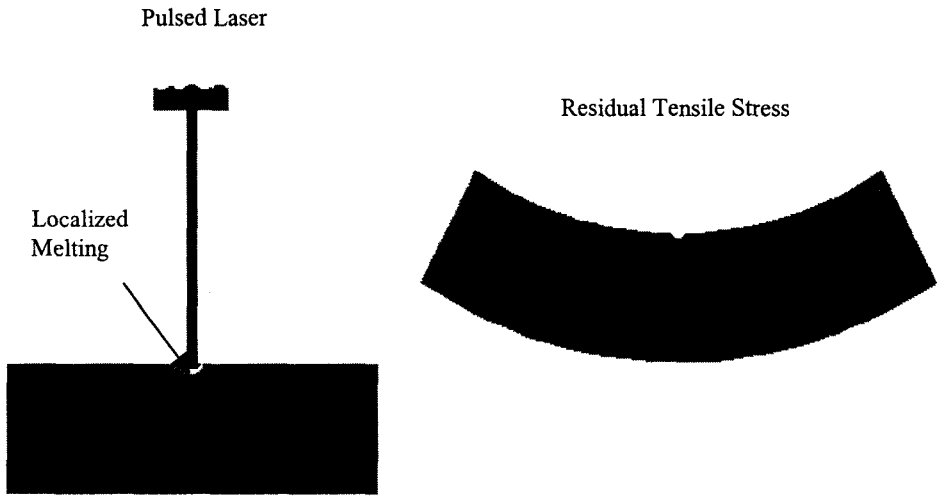

Figure 1. Laser Scribing Process

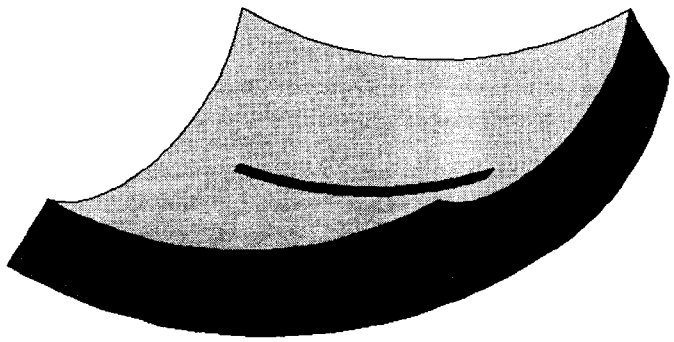

Figure 2. Illustration of Laser Scribe Slider

Forty-four sliders are attached along the 1.25mm edge, resulting in a 47mm by 1.25mm by 0.3mm *row* (shown in Figure 3). The two large surfaces are known as the air bearing surface (ABS side) and the flex side. The ABS side flies over the surface of the storage disk, while all scribing is performed on the flex side. The shape of the ABS side determines the flying height, so each slider's ABS side is measured while the flex side is scribed. The out of plane deflection w, of the ABS side is fitted with a bi-quadratic curve as follows:

$$w = f(x,y) = C_0 + C_1x + C_2y + C_3x^2 + C_4y^2 + C_5xy \quad (1)$$

where x and y and z are defined in Figure 4. The biquadratic curve fit assumes a constant curvature in x and y direction. The first three coefficients describe the best-fit plane through the surface (thus removing any rigid body rotations from the data). The final three coefficients define curvatures that are important in the aerodynamics that determine the flying height. These curvatures are normalized and defined as crown, camber, and twist:

$$Crown = -C_4L^2/4 \quad (2)$$

$$Camber = -C_3W^2/4 \quad (3)$$

$$Twist = -C_5LW \quad (4)$$

where L and W are the length and width of the ABS side (L = 1mm, W = 1.25 mm).

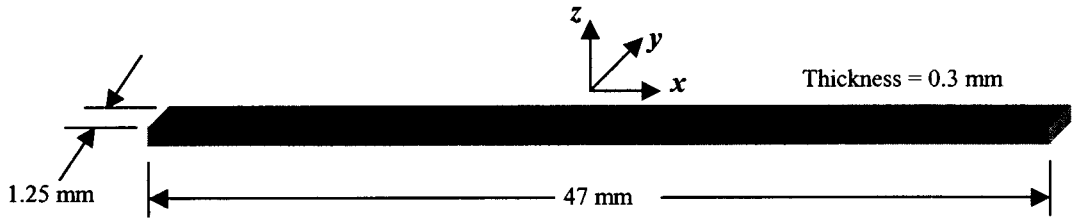

Figure 3. Row of Sliders

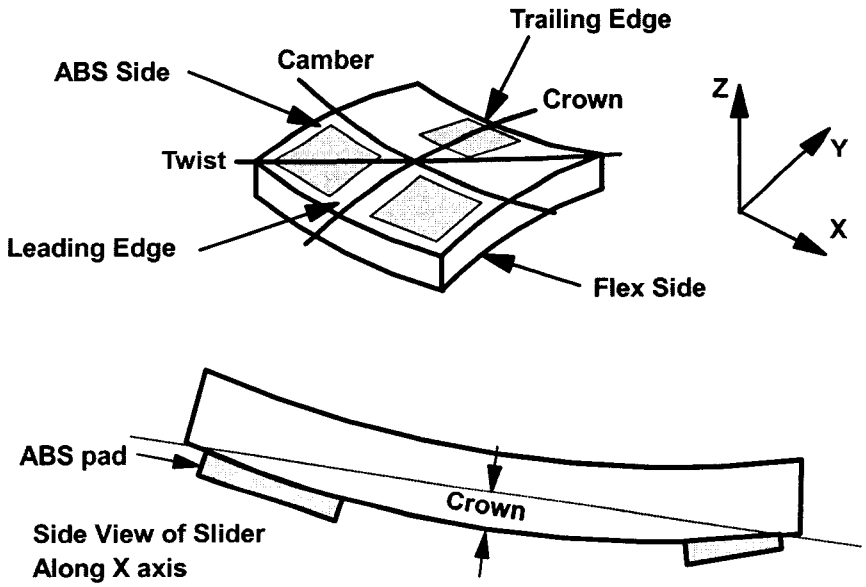

Figure 4. Slider Coordinate System and Curvature Definitions

The negative signs define positive curvature as curvature that lift the corners away from the storage disk. Figure 4 shows a graphical representation of crown, camber, twist, and the coordinate system. Note that in this diagram, crown is positive and camber is negative. Crown is the primary influence on slider flying height, but

control over camber and twist is essential for performance improvement. Currently, crown can be controlled accurately with the LCAT system—usually, to the nearest nanometer. The asymmetry represented by twist is a major problem in slider construction; in fact, one of the major objectives of this project is to develop scribing patterns to remove twist from a slider. The constants (C_1 - C_5) in biquadratic curve equation (1) are obtained by a least squares procedure, which provides the best fit to the out-of-plane deflections generated by the finite element models and the actual experiments at a finite number of points on the entire plate. The mean square error Er for the out-of-plane deflections in the entire plate can be written,

$$E_r = \sum_{i=1}^{N} (W_i - \omega_i)^2 \tag{5}$$

The symbol N indicates the number of the points where the deflections are specified in the entire plate. *Wi* is experimental or finite element analysis results at the specified coordinate. ω_i is the value from the biquadratic curve equation at the specified coordinate. Following standard least squares procedures, Er is minimized by enforcing the following conditions,

$$\frac{\partial E_r}{\partial C_0} = \frac{\partial E_r}{\partial C_1} = \frac{\partial E_r}{\partial C_2} = \frac{\partial E_r}{\partial C_3} = \frac{\partial E_r}{\partial C_4} = \frac{\partial E_r}{\partial C_5} = 0 \tag{6}$$

Imposing these conditions (6) yields a system of linear algebraic equations in the form of **Ax=b** that can be solved for the constants (C_1 through C_5). **A**,**x** and **b** are written in (7).

(7)

$$A = \begin{pmatrix} N & \sum_i x_i & \sum_i y_i & \sum_i x_i^2 & \sum_i y_i^2 & \sum_i x_i y_i \\ \sum_i x_i & \sum_i x_i^2 & \sum_i x_i y_i & \sum_i x_i^3 & \sum_i x_i y_i^2 & \sum_i x_i^2 y_i \\ \sum_i y_i & \sum_i x_i y_i & \sum_i y_i^2 & \sum_i x_i^2 y_i & \sum_i y_i^3 & \sum_i x_i y_i^2 \\ \sum_i x_i^2 & \sum_i x_i^3 & \sum_i x_i^2 y_i & \sum_i x_i^4 & \sum_i x_i^2 y_i^2 & \sum_i x_i^3 y_i \\ \sum_i y_i^2 & \sum_i x_i y_i^2 & \sum_i y_i^3 & \sum_i x_i^2 y_i^2 & \sum_i y_i^4 & \sum_i x_i \\ \sum_i x_i y_i & \sum_i x_i^2 y_i & \sum_i x_i y_i^2 & \sum_i x_i^3 y_i & \sum_i x_i y_i^3 & \sum_i x_i^2 y_i^2 \end{pmatrix} \quad X = \begin{Bmatrix} C_0 \\ C_1 \\ C_2 \\ C_3 \\ C_4 \\ C_5 \end{Bmatrix} \quad b = \begin{Bmatrix} \sum_i \omega_i \\ \sum_i x_i \omega_i \\ \sum_i y_i \omega_i \\ \sum_i x_i^2 \omega_i \\ \sum_i y_i^2 \omega_i \\ \sum_i x_i y_i \omega_i \end{Bmatrix}$$

Once the coefficients are known, computing curvature parameter (crown, camber. and twist) in the plate is a matter of evaluating the equations (2) through (4).

3. Experimental Scribing Results

In order to calibrate the model, several different sets of measurements were made using the laser scribing system and interferometer. The sliders are measured and scribed while still part of a row—making handling much simpler and requiring less complicated fixtures and shorter set up times. Currently, sliders are scribed and measured in a closed-loop system, described in more detail by Tam (Tam, et. al. (1999)). To measure the effects of laser scribes on sliders, an accurate determination of the shape of the slider before and after scribing is necessary. A laser (phase shift) interferometer (specifically, Wyko HD-2000) was used to determine the shape of the slider—its high resolution and non-contact measurement allows the slider to be measured with the required degree of precision.. To test the effect of a scribe pattern, an entire row was measured using the interferometer, then scribed, and the row was measured again. Subtracting the two slider profiles (before and after) gives the distortion generated by the scribes. Due to the high degree of precision necessary in the measurement of the sliders, the repeatability of the measurements must be considered when collecting data. To test the interferometer, curvatures from six sliders were recorded and the sliders were removed from the interferometer.

Some time later the sliders were measured again without any modifications. Table 1 shows the results of this test. The average repeatability of a single measurement is 0.098 nm. The scribing patterns used to calibrate the laser scribing model needed to encompass the LCAT's range of capabilities in scribe length, scribe location, and

scribe direction. There are a few limitations on scribe placement and length. The scribes cannot cross—interaction effects create problems with the surface of the slider. The scribes are approximately 40 μm wide;

placing an ultimate limit on scribe spacing. Also, the scribes cannot be placed too close to the edges of the slider—one edge contains the read/write electronics which are distorted by the residual stress induced by the laser scribes. To prevent creating additional twist, scribes are usually made in the x and y directions and are symmetric with respect to the other axis. Using multiple scribes for calibration raises the issue of superposition. Fortunately, a test for superposition is relatively simple; it consists of three patterns—two independent patterns and a pattern that contains all of the scribes present in the other two. If the curvatures of the "superposed" pattern are the sum of the curvatures of the two independent patterns, then superposition is obeyed. This exact test was performed and the results confirmed that laser scribing obeys superposition for non-overlapping scribes (see Figure 5-6). Since the scribes obey superposition, individual scribes can be modeled and their curvatures added to give the curvature generated by a certain scribing pattern—a versatile technique that allows a library of single-scribe solutions to represent a multitude of scribing patterns.

The set of experiments used for calibration purposes must give an accurate indication of the range of capability of the LCAT system and must be simple enough to model accurately. To accomplish this, all scribes were made in the x and y directions and were centered on the slider. Therefore, all of the calibration scribing patterns are symmetric with respect to the x and y axes, thus theoretically eliminating any twist generation. To encompass the range of ability of the LCAT system, the patterns must show variation in scribe length and placement. For scribes in the y direction, the length can vary from approximately 600 μm to 1000 μm. Note that test cases 6, 7, and 8 constitute a superposition test. This set of test cases encompasses a wide range of the LCAT's capabilities and provides adequate information to calibrate the model. Most of the scribe patterns were repeated for 11 sliders and the results were averaged to help reduce measurement repeatability errors in the calibration data. Results are shown in Figures 5 and 6 and more detailed results are given in Table 2.

Table 1. Interferometer Repeatability Test

Row No.	Slider No.	Crown Change (nm)	Camber Change (nm)	Twist Chang (nm)
1	10	-0.08	-0.03	0.18
1	20	0.12	-0.09	-0.09
3	10	-0.11	0.16	-0.12
3	20	0.07	-0.04	0.06
4	10	0.06	0.11	-0.17
4	20	0.05	0.14	-0.08

Table 2. Experimental Laser Scribing Data

		Curvature - Average			**Curvature-Standard Deviation**		
Test Case	No.Samples	Crown(nm)	Camber(nm)	Twist(nm)	Crown(nm)	Camber(nm)	Twist(nm)
1	8	1.6464	2.6527	-0.05	0.1726	0.1764	0.1998
2	10	1.8230	2.5480	0.0910	0.1739	0.0991	0.0700
3	11	1.6573	1.9600	-0.2127	0.1106	0.0822	0.1761
4	11	1.5800	2.5373	0.0155	0.1254	0.0940	0.2267
5	11	1.5573	1.8273	-0.0345	0.0855	0.0413	0.1882
6	7	1.9114	2.3457	0.0571	0.0871	0.0640	0.1751
7	7	2.8414	2.9443	-0.1514	2.5020	0.1336	0.3235
8	7	4.6371	5.3686	-0.5314	0.3661	0.2746	0.3321

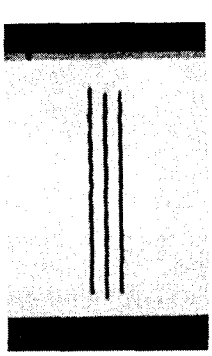

Test Case 1
3 *y* scribes
L = 1000 μm
Spacing = 80 μm
Crown: 1.65 nm
Camber: 2.65 nm
Twist: -0.05 nm

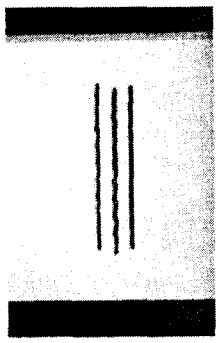

Test Case 2
3 *y* scribes
L = 800 μm
Spacing = 80 μm
Crown: 1.82 nm
Camber: 2.55 nm
Twist: 0.09 nm

Test Case 3
3 *y* scribes
L = 600 μm
Spacing = 80μm
Crown: 1.66 nm
Camber: 1.96 nm
Twist: 0.21 nm

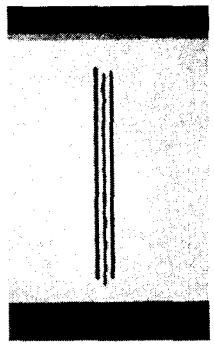

Test Case 4
3 *y* scribes
L = 1000 μm
Spacing = 40 μm
Crown: 1.58 nm
Camber: 2.54 nm
Twist: 0.02 nm

Figure 5. Experimental Results for Test Cases 1 through 4

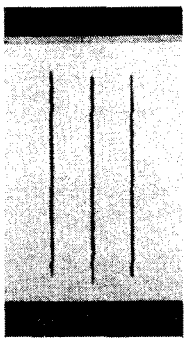

Test Case 5
3 *y* scribes
L = 1000 μm
Spacing = 240 μm
Crown: 1.56 nm
Camber: 1.83 nm
Twist: -0.03 nm

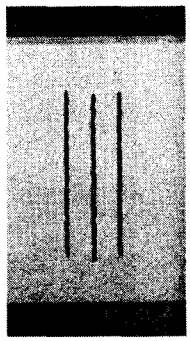

Test Case 6
3 *y* scribes
L = 800 μm
Spacing = 160 μm
Crown: 1.91 nm
Camber: 2.35 nm
Twist: 0.06 nm

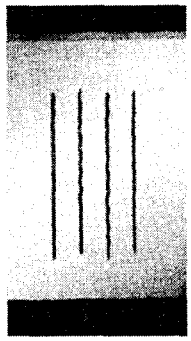

Test Case 7
4 *y* scribes
L = 800 μm
Spacing = 160 μm
Crown: 2.84 nm
Camber: 2.94 nm
Twist: -0.15 nm

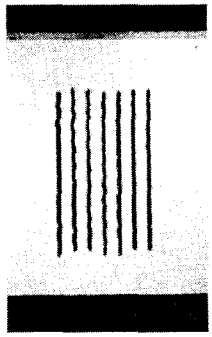

Test Case 8
7 *y* scribes
L = 800 μm
Spacing = 80 μm
Crown: 4.64 nm
Camber: 5.37 nm
Twist: -0.53 nm

Figure 6. Experimental Results for Test Cases 5 through 8.

Examination of the data reveals some interesting conclusions (both about metrology and the scribing results). The standard deviations are on the order of 0.10 nm —very close to the uncertainty predicted by the repeatability experiment, meaning that the laser scribes themselves are consistent and repeatable within the measurement error. The presence of small amounts of twist in the data indicates that the scribes may not have been completely symmetric with respect to the *x* and *y* axes or the scribing geometry is not as simple as once thought..

The inconsistent data from the end of the rows is a result of varying boundary conditions—the sliders in the middle of the row have other sliders (with similar scribing patterns) on both sides, but the sliders on the end have a free edge. The different boundary conditions can cause inconsistency in results—a point further demonstrated by the finite element models used to model the laser scribing. However, the experimental data does show that the laser scribing process is consistent and relatively repeatable across the range of operation of the LCAT system. Therefore, the experiments represent a good calibration set for the laser scribing model.

4. Finite Element Modeling

4.1 Boundary Conditions

One major consideration during the development of any finite element model is the boundary conditions. In this particular case, the actual sliders are scribed as a row, and the row itself has no obvious constraints. So, the boundary conditions placed on the finite element model must eliminate all of the rigid body motions (translations and rotations) but not over-constrain the model (such that the boundary conditions influence the solution). To accomplish this task, a set of boundary conditions known as a Kelvin coupling is employed. Figure 8 shows the coupling as a theoretical model. Point 1 is restrained from translation in all three directions, point 2 is restrained in y and z, and point three is restrained in z. This set of boundary conditions restrains the body from all six rigid body motions but allows the body to elastically deform without causing any stress. These no-stress boundary conditions are critical in accurately modeling the scribed sliders, so the Kelvin coupling is used on all of the finite element models used in this project.

4.2 Laser Scribe Force Specification

The experimental results in Section 3 show that laser scribes generate curvature parallel and perpendicular to the scribe. To model these deflections created by laser scribing, the line-dipole force model used in mechanical scribe case by Austin and Scattergood was implemented with some modification. The line dipole solution modeled the mechanical scribe as two set of line forces separated by a small distance. However, for the mechanical scribe case, the scribe produced curvature perpendicular to the scribe, but not parallel to the scribe. So, to produce this parallel curvature as seen in the laser scribe, a set of forces parallel to the scribe was added.

The force model with concentrated forces at the end of the scribe was developed for the laser scribe. Since force model has loads in both x and y directions on the surface, the elasticity theory is not a practical way to solve this problem. However, the load transfer is effected by a residual tensile force (P_x) on the scribed surface as shown in Fig. 9(a). The residual tensile force (P_x) can be converted to a equivalent force/moment referred to the centroidal axis of the plate as shown in Fig. 9(b).

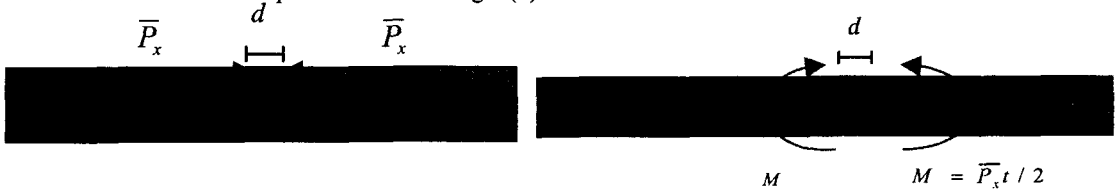

Figure 9a. Surface Dipole Force **Figure 9b.** Centroidal Dipole Force/Moment
Figure 9. Load Transfer Mechanism and equivalent Force/ Moment System

Scribing patterns matching those performed experimentally were modeled using the end force systems. The scribe region is 0.25 mm wide, with 24 elements spanning its width. Four elements are placed between the line forces, giving a dipole separation of 50 μm. There are 20 elements across its width, allowing scribes of 600, 800 and 1000 μm (three scribe lengths used in the experiments) to be modeled easily. Figure 10 shows the finite element model with the 1000 μm scribe. Note the coarse mesh outside of the scribe region—reducing the sze of the model without impacting the accuracy of the solution.

5. Finite Element Analysis Results

5.1 Calibration for the shape of the slider

The end force systems were applied to the finite element model using the following guidelines. The line dipoles were applied with 50 μm spacing, with a magnitude of f_M = 20 N/mm. The magnitudes of the end forces (F_m) were varied until the crown to camber ratio of a specific model matched that of the experimental results to a reasonable degree of precision. The modulus of elasticity was taken to be E =1 N/mm^2(the results, however, can be scaled linearly) and Poisson's ratio was taken to be 0.2. The model used for calibration is Test Case 1,consisting of three 1000 μm, y-direction scribes with a spacing of 80 μm. The experimental results gave a

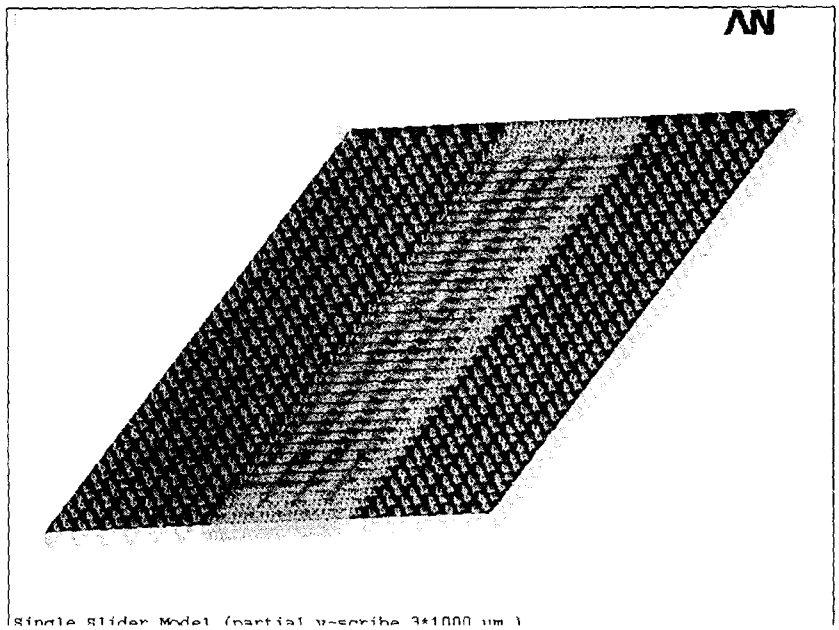

Figure 10. Finite Element Mesh for 1000 μm 3y Scribe

crown of 1.65 nm and 2.65 nm of camber, for a crown to camber ratio of 0.623. Varying the end force F_m in the end force model, gave a crown to camber ratio of 0.638 for Test Case 1 (a 2.44 % error) with $F_m \approx 0.656$ N/mm. Using this end force as the calibration, Test Cases 2 through 8 were computed using similar models. The results are shown in Table 4. The results show that the end force model is quite accurate for modeling the y-direction scribes—over all eight of the test cases, the maximum error is less than five percent.

5.2 Calibration for Deflection

The calibrations so far have not addressed the actual magnitude of the curvatures. Theoretically, this is a simle matter- the finite element analyses are linear, so the results can be scaled linearly to reflect changes in material properties and loading.

Creating the deflections requires the introduction of a multiplier constant(called C in the following analyses0 that scales the results of the finite element analyses to match the experimental results. The constant C was varied until the experimental and predicted camber for Test Case 1 were equal, resulting in C=55.8373. The other curvatures were normalized using the value, giving the data shown in Table 5. The errors shown for the magnitude calibration are much greater than those shown by the shape calibration –the average error for the y-scribe is 13.74 %.

Table 3. End Force System Calibration for *y*-scribing Models

	Finite Element Model			Experimental	
Test Case	Crown	Camber	Ratio	Ratio	% error
1	0.0303	0.0475	0.638	0.623	2.44
2	0.0290	0.0388	0.747	0.714	4.58
3	0.0254	0.0300	0.847	0.847	0.05
4	0.0305	0.0490	0.622	0.622	-0.07
5	0.0284	0.0330	0.862	0.852	1.19
6	0.0273	0.0336	0.815	0.813	0.27
7	0.0361	0.0389	0.928	0.966	-3.90
8	0.0635	0.0725	0.876	0.864	1.38

The substantial errors shown by the full calibrations could have several sources of origin—variation in the AlTiC between rows and variations in scribing parameters such as laser power and instrumentation drift could cause reasonable error. However, the errors do show a general trend—the error appears to be a function of length . In Table 5, the data is calibrated off of Test Case 1 (three 1000μm scribes with 80μm spacing), and the errors for the other 1000μm scribe cases (Test Cases 4 and 5) are reasonable. The 800μm scribe cases (Test Cases 2, 6, 7, and 8) show similar magnitudes of error, and the lone 600μm scribe case shows slightly more error than the 800μm scribe case. This trend suggests that making the calibration factor C a function of length could greatly improve accuracy.

To simplify the determination of the scaling factor, a linear fit was placed on each of the data sets, producing two equations for the scaling factor as a function of scribe length. A linear curve was chosen to illustrate the general trend because the lack of data prevents a higher order polynomial or function curve-fit. The two equations are shown below.

$$C_y(L) = -0.03\,L + 87$$

Using these equations to generate the scaling factors for the test cases, the finite element results were calibrated and compared to the experimental results, resulting in the data shown in Table 6. Note the improvement in accuracy over the calibrations shown in Tables 5 and 6—the average error for all 8 test cases is 9.05%, with a maximum error of 16.73%.

Table 4. Full Calibration for y-scribes ($C = 0.04342$)

	Crown			Camber		
Test Case	Experimental	Predicted	% error	Experimental	Predicted	% error
1	1.646	1.646	2.86	2.653	2.653	0.00
2	1.823	1.823	-11.10	2.548	2.170	-14.82
3	1.657	1.657	-14.28	1.960	1.676	-14.49
4	1.580	1.580	7.83	2.537	2.741	8.03
5	1.557	1.557	2.18	1.827	1.845	1.00
6	1.911	1.911	-19.95	2.346	1.877	-20.01
7	2.841	2.841	-29.00	2.944	2.173	-26.20
8	4.637	4.637	-23.51	5.369	4.049	-24.58

Table 5. Calibrated Results Using Scribe Length Dependent Scaling Factor Model

Test Case	Scaling Factor	Predicted Crown	% error	Predicted Camber	% error
1	57	1.728	5.0	2.708	2.08
2	63	1.828	0.3	2.449	-3.90
3	67	1.755	5.93	2.071	5.67
4	57	1.739	10.07	2.798	18.71
5	57	1.624	4.3	1.884	3.10
6	63	1.726	-9.68	2.117	-9.75
7	63	2.276	-19.9	2.451	-16.73
8	63	4.002	-13.7	4.569	-14.91

References

1. Ahn, Y.,T. N. Farris, and S. Chandraskar, "Elastic Stress Fields Caused by Sliding Micro-indentation of Brittle Materials," Proceedings of the International Conference On Machining of Advanced Materials, S. Jahanimir, ed., NIST Special Publication 847, 1993.

2. Austin, Brad, Masters Thesis, North Carolina State University, 2000.
3. Liu, D.M., et. al., "Laser-induced Deformation on a Hard Disk Surface," Applied Surface Science, Volume 138-139, 1999,p.482-488
4. Tam, A.C., C.C. Poon, L. Crawforth, and P.M. Lundquist, "Manufacturing: Stress on the Dotted Line," IBM Publications, Almaden Research Center, Volume 6, 1999, Issue 13,
5. Yoffe, E.H.,"Elastic Stress Fields Caused by Indenting Brittle Materials," Phil. Mag. A, Volume 46, No. 4, 1982.